The Astrophysical Journal, 647:L65–L68, 2006 August 10

THE ROLE OF INTERPLANETARY SCATTERING IN WESTERN HEMISPHERE LARGE SOLAR ENERGETIC PARTICLE EVENTS

G. M. Mason,[1] M. I. Desai,[2] C. M. S. Cohen,[3] R. A Mewaldt,[3] E. C. Stone,[3] and J. R. Dwyer[4]
Received 2006 June 16; accepted 2006 July 6; published 2006 August 1

ABSTRACT

Using high-sensitivity instruments on the *ACE* spacecraft, we have examined the intensities of O and Fe in 14 large solar energetic particle events whose parent activity was in the solar western hemisphere. Sampling the intensities at low (~273 keV nucleon^{-1}) and high (~12 MeV nucleon^{-1}) energies, we find that at the same kinetic energy per nucleon, the Fe/O ratio decreases with time, as has been reported previously. This behavior is seen in more than 70% of the cases during the rise to maximum intensity and continues in most cases into the decay phase. We find that for most events if we compare the Fe intensity with the O intensity at a higher kinetic energy per nucleon, the two time-intensity profiles are strikingly similar. Examining alternate scenarios that could produce this behavior, we conclude that for events showing this behavior the most likely explanation is that the Fe and O share similar injection profiles near the Sun, and that scattering in the interplanetary medium dominates the profiles observed at 1 AU.

Subject headings: acceleration of particles — cosmic rays — interplanetary medium — Sun: abundances — Sun: flares

1. INTRODUCTION

When the first detailed observations of heavy elements in solar energetic particle (SEP) events were made in the 1970s, it was discovered that the Fe intensity reached its maximum before O at the same kinetic energy per nucleon (O'Gallagher et al. 1976; von Rosenvinge & Reames 1979; Mason et al. 1983). Later studies of the time to maximum for Fe, O, and other species, as well as decay time constants, have shown that in many SEP events the differences in temporal behavior are systematically ordered by particle species (Dietrich & Tylka 2001; Sollitt et al. 2003). The differences in temporal behavior were attributed to the different magnetic rigidity of Fe versus O, which is due to the partial stripping of ions in SEP events, for example, $(M/Q)_{\rm Fe} = 4.8$ while $(M/Q)_{\rm O} = 2.4$ (Klecker et al. 2000; Möbius et al. 2000).

However, it was not clear which physical mechanisms were responsible for this behavior. For example, Scholer (1976) and Mason et al. (1983) fitted their observations assuming identical injections at the Sun followed by scattering in the interplanetary medium (IPM), including effects of diffusion, convection, and adiabatic deceleration. On the other hand, Mason et al. (1991) showed that two SEP events well fitted at 1 AU using effects of interplanetary propagation could be equally well fitted assuming that the injection at the Sun was extended over a long period followed by nearly scatter-free propagation in the interplanetary medium. Thus, it remains unclear whether the different temporal behavior of these species was due to the acceleration-release process, interplanetary propagation, or some combination of these.

Recent advances in numerical modeling of SEP events associated with coronal mass ejections (CMEs) feature routine inclusion of details of the particle acceleration at the shock followed by interplanetary propagation after particles escape the acceleration region. In some cases, the particles undergo significant scattering in the IPM (e.g., Ng et al. 1999; Li et al. 2005), while in others the transport is nearly scatter-free (Lee 2005). Although solutions from all these models show properties qualitatively similar to the observations, it remains unclear whether the simulated acceleration versus transport effects accurately reflect the processes in large SEP events.

In this Letter, we investigate this issue by examining the temporal behavior of SEP O and Fe over a broad energy range in large SEP events, and we conclude that scattering in the IPM plays a crucial role in a majority of the cases.

2. OBSERVATIONS

The observations reported here were carried out with the Ultra Low Energy Isotope Spectrometer (ULEIS; Mason et al. 1998) and the Solar Isotope Spectrometer (SIS; Stone et al. 1998) on the *Advanced Composition Explorer* (*ACE*) spacecraft, which was launched into an orbit around the sunward Lagrangian point in 1997. ULEIS is a time-of-flight mass spectrometer covering the energy range ~0.1–10 MeV nucleon^{-1}. SIS is a dE/dx versus residual energy spectrometer covering the range ~6–160 MeV nucleon^{-1}.

In order to survey typical SEP event properties, we first chose all the events in the NOAA Space Environment Center list of >10 MeV SEP proton events between the launch of *ACE* and 2005 January.[5] All these events were associated with shocks or CMEs. In order to minimize effects arising from magnetic connection, we kept only events with parent activity in the western hemisphere and also discarded events complicated by multiple CMEs (e.g., 1997 November and 2000 July). The resulting group of 14 "simple" SEP events is listed in Table 1.

Figure 1 (*left*) shows O and Fe time-intensity profiles at low (273 keV nucleon^{-1}) and high (~12 MeV nucleon^{-1}) energies for event 1. The reasonably prompt rise is typical, but note that at low energies the profile is more complex than a simple rise to maximum and decay (this is typical at low energies). Note also that both Fe and O rise at about the same time, and then

[1] Applied Physics Laboratory, Johns Hopkins University, 11100 Johns Hopkins Road, Laurel, MD 20723; glenn.mason@jhuapl.edu.
[2] Southwest Research Institute, 6220 Culebra Road, San Antonio, TX 78238.
[3] Space Radiation Laboratory, California Institute of Technology, Mail Code 220-47, 1200 East California Boulevard, Pasadena, CA 91125.
[4] Department of Physics and Space Sciences, Florida Institute of Technology, 150 West University Boulevard, Melbourne, FL 32901.

[5] See http://solar.sec.noaa.gov/ftpdir/indices/SPE.txt.

TABLE 1
14 Western Hemisphere Large SEP Events

Event No.	Year	Flare			Peak Proton Flux[a]	Event-averaged Fe/O[b]	*E*-Ratio Low[c]	*E*-Ratio High[d]
		Maximum	X-Ray Class/Importance	Location				
1	1998	Sep 30, 13:50	M2/2N	N23, W81	1200	0.195 ± 0.006	2.0	1.9
2	1999	Jun 4, 07:03	M3/2B	N17, W69	64	1.063 ± 0.027	1.4	1.0
3	2000	Sep 12, 12:13	M1/2N	S17, W09	320	0.290 ± 0.007	2.0	1.9
4	2000	Oct 25, 11:25	M2[e]	W50[e]	15	0.215 ± 0.007	1.0	Stat.[f]
5	2001	Jan 28, 16:00	M1/1N	S04, W59	49	0.274 ± 0.007	2.0	1.9
6	2001	Apr 15, 13:50	X14/2B	S20, W85	951	1.325 ± 0.047	2.0	1.4
7	2002	Apr 21, 01:51	X1/1F	S14, W84	2520	0.752 ± 0.043	2.8	3.9
8	2002	Jul 7, 11:43	M1	West limb	22	0.028 ± 0.002	1.4	Stat.[f]
9	2002	Aug 14, 02:12	M2/1N	N09, W54	26	0.253 ± 0.009	2.0	Irr.[g]
10	2002	Aug 24, 01:12	X3/1F	S08, W90	317	0.536 ± 0.014	Irr.[g]	1.9
11	2003	Nov 4, 19:29	X28/3B	S19, W83	353	1.217 ± 0.030	2.8	1.0
12	2003	Dec 2, 09:48	C7	West limb	86	0.887 ± 0.022	2.0	Stat.[f]
13	2004	Apr 11, 04:19	C9/1F	S14, W47	35	0.316 ± 0.010	2.0	1.9
14[h]	2005	Jan 20, 07:01	X7.9	N14, W61	1860	0.261 ± 0.021	2.8	1.9

[a] In units of particles s^{-1} cm^{-2} sr^{-1} above 10 MeV.
[b] At 0.32–0.45 MeV $nucleon^{-1}$ (Desai et al. 2006).
[c] Ratio of O kinetic energy per nucleon to Fe at 276 keV $nucleon^{-1}$ to give a time-invariant ratio.
[d] Ratio of O kinetic energy per nucleon to Fe at 13.2 MeV $nucleon^{-1}$ to give a time-invariant ratio.
[e] Flare identification from Kahler (2005).
[f] The statistical accuracy is insufficient to compare intensities accurately.
[g] Irregular temporal variation of the Fe/O ratio precluded finding the energy (if any) at which Fe/O was time-invariant.
[h] Last in a sequence of three events that occurred between 2005 January 16 and January 20.

O continues to rise even after the Fe has begun to decay. This behavior produces the decreasing Fe/O ratio mentioned earlier.

The right panel of Figure 1 shows the same Fe time-intensity profiles, with O profiles taken at a higher kinetic energy per nucleon (the ratios of the higher O energies to Fe selected for each event are given in the rightmost columns of Table 1). The O profiles are strikingly similar to the corresponding Fe profiles. This is especially surprising during the rise phase for the low-energy data, since the 546 keV $nucleon^{-1}$ O has a scatter-free travel time to 1 AU about 2 hr shorter than the 273 keV $nucleon^{-1}$ Fe, a difference that would be easily visible in the figure. (For the high-energy data, the difference in travel times is only ~15 minutes and so would not be visible.) Note that the similarity of the Fe intensity to the O intensity goes beyond a general similarity and holds even for some of the irregular features of the profiles.

Since particle intensities increase rapidly during the rise portion of these events, it is hard to tell whether the similarity between the rise-phase Fe and O is greater in the left versus the right panel of Figure 1. However, the ratio of Fe to O is a more sensitive indicator of the relative behavior of the two species. Figure 2*a* shows the Fe/O ratios for event 1, with the left panel showing the ratios at the same energy per nucleon (as in Fig. 1, *left*) and the right panel showing the ratios with higher energy per nucleon O (as in Fig. 1, *right*). The large filled circles mark the time of maximum of the Fe intensity. Note that at the same energy per nucleon the Fe/O ratio decreases by an order of magnitude, changing fairly smoothly from the onset and continuing through and well beyond the time of maximum. For the ratio of Fe with higher energy O (Fig. 2*a*, *right*), the systematic decrease of the ratio is gone, and only fluctuations around a nearly constant value remain.

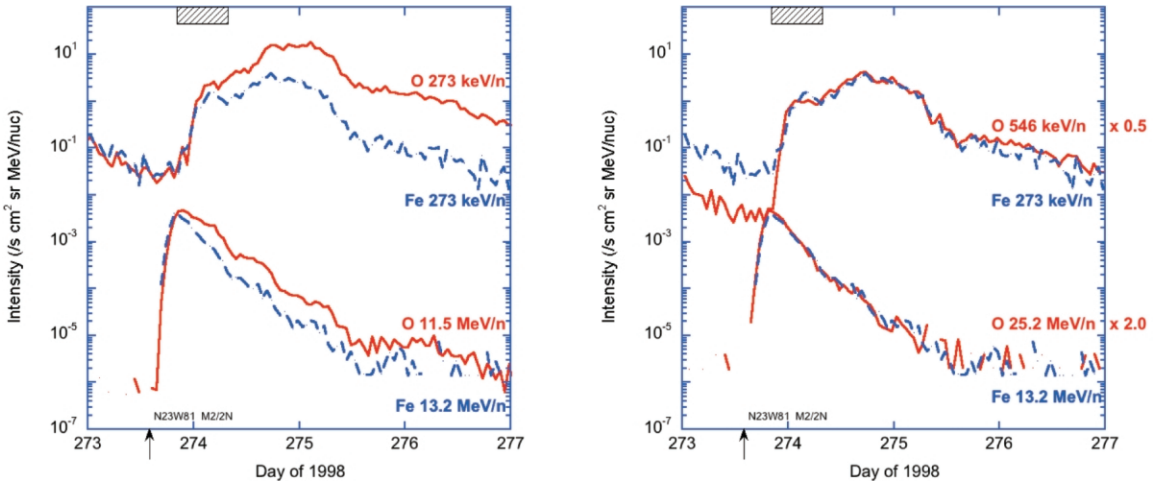

Fig. 1.—*Left*: Oxygen (*solid red line*) and iron (*dashed blue line*) hourly average intensities at 237 keV $nucleon^{-1}$ and ~12 MeV $nucleon^{-1}$ for event 1; the hatched box shows the duration of large anisotropies at low energy. *Right*: Same as the left panel for Fe intensity; the O intensities are at approximately twice the kinetic energy per nucleon as the left panel and renormalized as shown to facilitate comparison with Fe intensity.

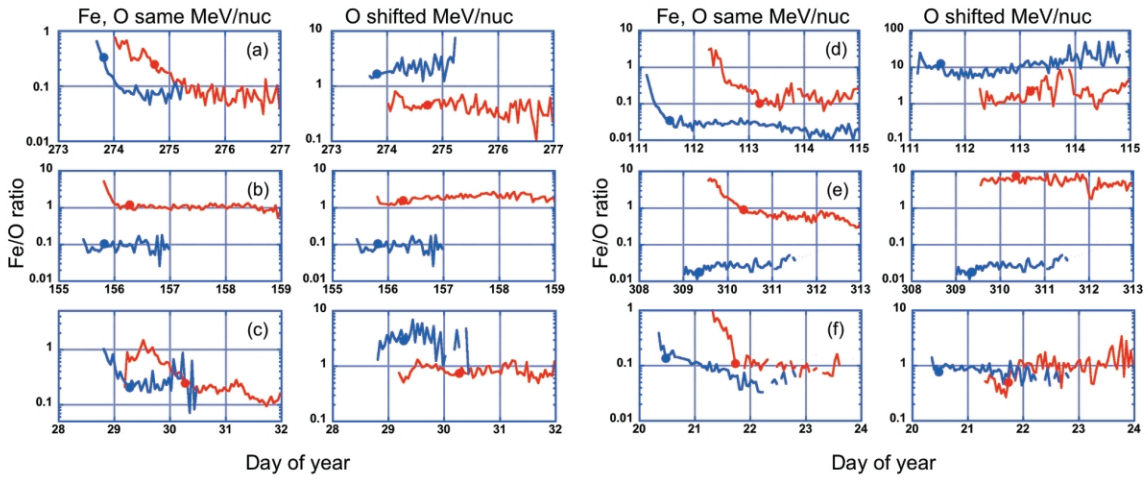

FIG. 2.—*Left panels*: Fe/O ratio at 273 keV nucleon^{-1} (*red*) and ~12 MeV nucleon^{-1} (*blue*), for (*a*) event 1, (*b*) event 2, (*c*) event 5, (*d*) event 7, (*e*) event 11, and (*f*) event 14. *Right panels*: The same events, Fe/O ratio with Fe at same energy as before, and O at a higher energy given by the factor shown in Table 1. Large filled circles mark the time of maximum intensity of Fe. Late times of maximum at 273 keV nucleon^{-1} for some events (e.g., [*c*], [*d*], [*f*]) are due to intensity peaking at shock passage.

This is a reflection of the level of agreement between the time-intensity profiles in the right panel of Figure 1.

Figures 2*b*–2*f* show representative pairs of Fe/O ratios for other events in Table 1. Note that in most cases a large systematic decrease in the Fe/O ratio is replaced by a nearly constant Fe/O ratio when higher energy O is used. These nearly constant Fe/O ratios show that for these events, the Fe intensity profiles are similar to higher energy O profiles as in Figure 2 (*right*). In selecting higher energy O intensities to compare with Fe, we used standard energy bins that are spaced by a factor of 1.4 on ULEIS and ~1.9 on SIS. There are some other features of these panels that we note here:

1. In several cases (Figs. 2*b*, 2*d*, 2*e*, 2*f*, *left*) at the same energy per nucleon, the Fe/O ratio decrease continues only to the time of maximum and afterward is nearly constant.
2. In the case of Figures 2*b* and 2*e* (*left*), the lower energy data show a decrease in Fe/O, while the ~12 MeV nucleon^{-1} ratio is constant at the same Fe and O energies (denoted by an *E*-ratio of 1.0 in Table 1 and a repeat of the same energy Fe/O ratio in the right panels of Fig. 2).
3. The scatter is larger in the plots with higher energy O, mainly because of poorer counting statistics.

3. DISCUSSION

Twelve of the 14 events (see Table 1) show a reasonably flat Fe/O ratio after comparing the 276 keV nucleon^{-1} Fe with higher energy O, and eight of 11 events show such flattening for the 13 MeV nucleon^{-1} Fe compared with higher energy O. (Three events, Nos. 4, 8, and 12, had poor statistics at high energies, precluding a comparison.) Intermediate-energy comparisons fit smoothly into the pattern shown here, making these properties typical of large western hemisphere SEP events.

How do these features fit into the alternate acceleration-release versus propagation-dominated scenarios mentioned earlier? For the propagation-dominated case, we follow the recent discussion of Cohen et al. (2005 and references therein). If the release profiles at the source for Fe and O are similar, then for a given set of interplanetary conditions the intensities at 1 AU will be controlled by the diffusion coefficient: $\kappa = v\lambda/3$, where v is the particle speed and λ is the scattering mean free path (mfp). Typically, the mfp is a function of particle's magnetic rigidity, so $\lambda \propto (vM/Q)^{\alpha}$, where α is related to the interplanetary turbulence power spectrum. The similarity of the Fe and O profiles implies that their diffusion coefficients are the same, $\kappa_{\rm O} = \kappa_{\rm Fe}$, so substituting for λ above we deduce the ratio of kinetic energies per nucleon where this condition is met:

$$E_{\rm O}/E_{\rm Fe} = [(Q/M)_{\rm O}/(Q/M)_{\rm Fe}]^{2\alpha/(\alpha+1)}.$$

For the typical (M/Q)-values quoted above, the quantity in square brackets is 2.052, so we have

$$E_{\rm O}/E_{\rm Fe} = 2.052^{2\alpha/(\alpha+1)}.$$

Taking a simple average of the energy ratio values in Table 1, this implies $\alpha = 0.9 \pm 0.2$, comparable to recent theoretical estimates (e.g., Shalchi et al. 2004 and references therein). At tens of MeV per nucleon, the charge state of Fe is often higher than at low energies; for example, if we use high-energy O and Fe ionization states from Leske et al. (1995) or Cohen et al. (1999), the ratio $E_{\rm O}/E_{\rm Fe} \sim 1.4$–1.6, similar to some cases listed in Table 1. The exponent α may also vary from event to event, or even with energy per nucleon, so other factors could contribute to the different energy ratios in Table 1.

For the scenario of acceleration-release followed by nearly scatter-free propagation, the decrease of the Fe/O ratio at the same energy per nucleon would be due to the earlier escape of Fe from the scattering region near the shock. This occurs because its larger M/Q ratio gives Fe a larger scattering mfp, so it can reach the shock's upstream escape "boundary" more easily than O. The near-equality of the Fe versus higher energy O time-intensity profiles, however, is a coincidence in this scenario, since after escaping from the shock acceleration region O would propagate to 1 AU faster than the Fe. For example, the equality we see between Fe and O at 273 versus 546 keV nucleon^{-1} requires that the Fe release was 2 hr ahead of the O release, such that the two particle populations just crossed each other as they reached 1 AU. Similar matching would be required at other energies, for example, a 15 minute

difference at 10 MeV nucleon^{-1}. While this cannot be ruled out for any single event, it seems very unlikely to us that such a coincidence occurs in such a large fraction of the cases. We conclude that for events showing time-invariant Fe/O ratios for O with higher energy per nucleon than Fe, the most reasonable explanation is that the Fe and O have similar release profiles near the Sun followed by substantial scattering on the way to 1 AU.

Some of the events (e.g., No. 11) occurred during periods of high activity when turbulence could easily have been produced by CMEs, thus explaining the key role of scattering in the IPM. Others, however, occurred when there was little or no other obvious activity. Many of the events studied here are of a type in which electrons arrive promptly (Krucker & Lin 2000; Haggerty & Roelof 2002); also regarding the ions, the onset of event 14 was extremely fast from SIS energies to relativistic energies (see, e.g., Bieber et al. 2005). So how is it possible that interplanetary scattering plays such a key role in most of the MeV heavy-ion events studied here? In cases where there is no obvious source of turbulence, we note that all these events had elevated >10 MeV proton intensities, and that a possible explanation lies in the generation of proton-amplified waves generated by the streaming SEPs (Ng et al. 1999). The growth rate timescale for these waves is roughly an hour, so high-energy protons and near-relativistic electrons will begin to arrive at 1 AU before the waves have been amplified significantly, allowing prompt arrivals for electrons and high-energy protons and scattering-dominated profiles for the MeV ions.

Finally, it should be emphasized that the evidence for a critical role for interplanetary scattering presented here is not affected by whether the acceleration-release near the Sun is prompt or delayed; the only source requirement is that the Fe and O particle spectra at release are similar.

This work was supported by NASA grant NNG04GJ51G at the Johns Hopkins University Applied Physics Laboratory, NASA grant NAG 5-6912 and NSF grant ATM 04-54428 at the California Institute of Technology, and NASA grant NNG05GQ96G and NSF grant ATM 05-55878 at SwRI.

REFERENCES

Bieber, J. W., et al. 2005, Proc. 29th Int. Cosmic Ray Conf. (Pune), 1, 237
Cohen, C. M. S., et al. 1999, Geophys. Res. Lett., 26, 149
———. 2005, J. Geophys. Res., 110, A09S16, doi: 10.1029/2005JA011004
Desai, M. I., Mason, G. M., Gold, R. E., Krimigis, S. M., Cohen, C. M. S., Mewaldt, R. A., Mazur, J. E., & Dwyer, J. R. 2006, ApJ, in press
Dietrich, W. F., & Tylka, A. J. 2001, Proc. 27th Int. Cosmic Ray Conf. (Hamburg), 27, 3173
Haggerty, D. K., & Roelof, E. C. 2002, ApJ, 579, 841
Kahler, S. 2005, ApJ, 628, 1014
Klecker, B., et al. 2000, in AIP Conf. Proc. 528, Acceleration and Transport of Energetic Particles Observed in the Heliosphere, ed. R. A. Mewaldt et al. (Melville, NY: AIP), 135
Krucker, S., & Lin, R. P. 2000, ApJ, 542, L61
Lee, M. A. 2005, ApJS, 158, 38
Leske, R. A., Cummings, J. R., Mewaldt, R. A., Stone, E. C., & von Rosenvinge, T. T. 1995, ApJ, 452, L149
Li, G., Zank, G. P., & Rice, W. K. M. 2005, J. Geophys. Res., 110, A06104, doi: 10.1029/2004JA010600
Mason, G. M., Gloeckler, G., & Hovestadt, D. 1983, ApJ, 267, 844
Mason, G. M., Reames, D. V., & Ng, C. K. 1991, Proc. 22nd Int. Cosmic Ray Conf. (Dublin), 3, 197
Mason, G. M., et al. 1998, Space Sci. Rev., 86, 409
Möbius, E., et al. 2000, in AIP Conf. Proc. 528, Acceleration and Transport of Energetic Particles Observed in the Heliosphere, ed. R. A. Mewaldt et al. (Melville, NY: AIP), 131
Ng, C. K., Reames, D. V., & Tylka, A. J. 1999, Geophys. Res. Lett., 26, 2145
O'Gallagher, J. J., Hovestadt, D., Klecker, B., Gloeckler, G., & Fan, C. Y. 1976, ApJ, 209, L97
Scholer, M. 1976, ApJ, 209, L101
Shalchi, A., Bieber, J. W., Matthaeus, W. H., & Qin, G. 2004, ApJ, 616, 617
Sollitt, L. S., Stone, E. C., Mewaldt, R. A., Cohen, C. M. S., Leske, R. A., Widenbeck, M. E., & von Rosenvinge, T. T. 2003, Proc. 28th Int. Cosmic Ray Conf. (Tsukuba), 6, 3295
Stone, E. C., et al. 1998, Space Sci. Rev., 86, 357
von Rosenvinge, T. T., & Reames, D. V. 1979, Proc. 16th Int. Cosmic Ray Conf. (Kyoto), 5, 68